Surface Modification for Suppressing Interfacial Parasitic Reactions of Nickel-rich Lithium-Ion Cathode

Han Gao[1], Jiyu Cai[2], Gui-Liang Xu[1], Luxi Li[3], Yang Ren[3], Xiangbo Meng[2*], Khalil Amine[1, 4*], and Zonghai Chen[1*]

1. Chemical Sciences and Engineering Division, Argonne National Laboratory, Lemont, IL, USA, 60439
2. Department of Mechanical Engineering, University of Arkansas, Fayetteville, AR, USA, 72701
3. X-ray Science Division, Advanced Photon Source, Argonne National Laboratory, Lemont, IL, USA, 60439
4. Department of Materials Science and Engineering, Stanford University, Stanford, CA, USA 94305

Corresponding Authors

*X. Meng. Email: xbmeng@uark.edu.

*K. Amine. E-mail: amine@anl.gov.

*Z. Chen. E-mail: zonghai.chen@anl.gov.

Abstract

Ni-rich lithium nickel manganese cobalt oxides ($LiNi_xMn_yCo_{1-x-y}O_2$, $x \geq 0.5$, NMCs) are high capacity cathode materials for Li-ion batteries, but they exhibit limited cycling stability under high cut-off potentials. Various aspects, including transition metal dissolution, structural disordering, particle cracking, surface film thickening, and etc., have already been investigated for their performance degradation in the battery research community. Interestingly, these phenomena were primarily observed at the surface layer of the cathode material, implying that they may also be facilitated by some interfacial parasitic reactions between the delithiated NMC electrode and the non-aqueous electrolyte. In this study, $LiNi_{0.6}Mn_{0.2}Co_{0.2}O_2$ (NMC 622) electrodes chemically modified with TiO_2 via atomic layer deposition (ALD) were used as a model system to demonstrate the criticalness of the interfacial parasitic reactions. The suppression of the interfacial parasitic reactions effectively reduced the hike of cathodic surface film resistance, decreased the dissolution of transition metals, lowered the particle fragmentation, and mitigated the cation mixing of NMC 622. All these results demonstrated that careful design of the interfacial layer by surface modifications is a key approach to improve the durability of Ni-rich NMCs under high-voltage cycling.

Key words:

Li-ion batteries, Ni-rich cathode, parasitic reactions, interfacial reactions, surface modification

Graphical abstract

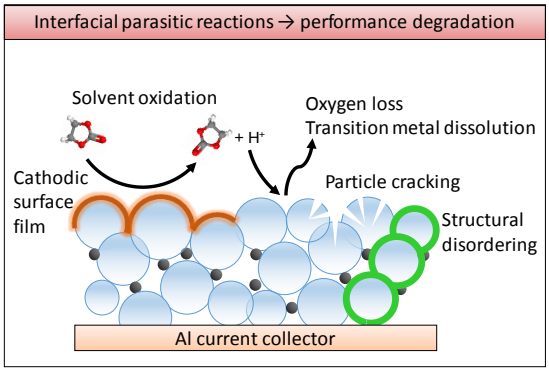

Introduction

Ni-rich lithium nickel manganese cobalt oxides ($LiNi_xMn_yCo_{1-x-y}O_2$, $x \geq 0.5$, NMCs) are high capacity cathode materials for Li-ion batteries.[1-3] However, they suffer from poor cycling stability at potentials above 4.3 V vs. Li/Li^+, which limits their available energy density. This degraded cyclability of Ni-rich NMCs are highly related to the parasitic reactions at their electrode/electrolyte interface, especially at high working potentials.

Generally, the parasitic reactions at the cathode interface include a series of complicated chemical reactions, mostly initiated by the electron transfer reaction between the cathode material and the electrolyte. Our pervious study shows that the parasitic reactions at a relatively lower potential (<4.5 V vs. Li^+/Li) is dominated by the chemical reaction between the delithiated cathode and the solvent while the parasitic reactions at a higher potential are dominated by the electrochemical oxidation of the solvent molecules.[2] Regardless of the chemical nature of the electron transfer reaction, both the electrochemical reaction and the chemical reaction lead to the oxidation of carbonate solvents and the deposition of side products at the cathode/electrolyte interface, causing a growth of the solid electrolyte interphase and large impedance hikes.[4-5] In addition, the oxidized solvent molecules (e.g. organic radical cations) are energetically unstable, and proton-bearing species will be generated and locally deposit at the interfacial layer of the cathode material. These reactions lead to a highly concentrated and localized H^+ and proton-bearing species at the positive electrode surface, [4, 6-8] deteriorating the electrochemical performance of the cathode materials. [4, 9-11]

Apparently, the partial loss of surface oxygen is somehow associated with the surface structural disordering of NMCs at high potentials. The increase in the transition metal element to oxygen atomic ratio leads to the irreversible migration of Ni cations to the Li layers (i.e. so-

called cation intermixing), forming electrochemically inactive NiO-type phase.[12-14] This ultimately results in a permanent phase transformation from layered structures to rock-salt and/or spinel-like structures.[15-17] In addition, the leaching out of transition metal cations will also reduce the number of active Li^+ host sites for the positive electrode and trap additional cyclable Li^+ on the surface of the negative electrode (i.e. chemical cross-talk in full-cells). Therefore, we believe it is essential to suppress the interfacial parasitic reactions between the delithiated NMC electrode and the non-aqueous electrolyte in order to improve the durability of Ni-rich NMCs for high-voltage cycling.

In this work, we report a systematic study on the interfacial parasitic reactions occurring in high-voltage Ni-rich NMC cells by using $LiNi_{0.6}Mn_{0.2}Co_{0.2}O_2$ (NMC 622) electrodes chemically modified with TiO_2 via atomic layer deposition (ALD). Unlike other simple coating methods, strong chemical bonds can be created between the central Ti atom of TiO_2 and the selected sites (the ones with naturally existing surface hydroxyl groups) of the NMC 622 substrate during the ALD process. In this way, the surface of the NMC 622 electrode can be chemically modified using sequential, self-limiting surface reactions. The purpose of this paper is to provide fundamental understandings and experimental evidence towards the suppression of parasitic reactions involving Ni-rich NMCs rather than focusing on the optimization around a specific chemistry. We used TiO_2, a well-known material for cathode protection[18-22], on NMC 622 as a model system to validate our proposed mechanisms and to demonstrate the effectiveness and benefits of our design philosophy. We will show that the suppression of the parasitic reactions by surface modification is an important approach to improve the cycling stability of NMC 622 by mitigating the undesired impedance growth, transition metal leaching, particle cracking, and cation mixing.

Experimental Section

Preparation of electrodes and cells

NMC electrode laminates were prepared by coating a slurry onto Al foil substrates using a doctor blade. The composition of the laminates was 91.5 wt. % NMC 622 (Ecopro Co., research grade with no surface coatings or doping), 4.4 wt. % carbon black (C45, Timcal), and 4.1 wt. % polyvinylidene fluoride (PVdF, Solvay). Graphite laminates were prepared by coating a slurry onto Cu foil substrates. The composition of the laminates was 92 wt. % graphite (MAGE, Hitachi), 2 wt. % carbon black, and 6 wt. % PVdF. All laminates were dried at 75 ºC in air overnight and calendered. Chemical modification with TiO_2 were performed on the NMC electrode laminates by ALD using titanium tetra-isopropoxide (TTIP, $Ti(OCH(CH_3)_2)_4$) and water as precursors[23] in a commercial ALD reactor (Savannah S200, Cambridge Nanotechnology Inc.) at 120 °C. Experimental details of the ALD process are included in the Supporting Information. Modified electrode samples are referred as ALD-x, where x represents the number of ALD cycles involved during the modification process.

All laminates were subsequently punched (14 mm in diameter for NMC and 15 mm for graphite). The NMC mass loading was ca. 20 mg per disk. CR2032 coin cells were constructed with Celgard 2325 separators and Li metal counter (for NMC half-cells) or graphite electrodes (for NMC/graphite full-cells, with an N/P ratio of ~1.2). All punched electrodes were vacuum-dried at ca. 110 ºC overnight prior to cell assembly. The electrolyte used was 1.0 M $LiPF_6$ in EC/EMC (3:7 by weight, LP-57, BASF).

Material and electrochemical characterizations

Microscopic images of the electrodes were obtained from a Hitachi S-4700-II field emission scanning electron microscope (SEM) coupled with a Bruker Energy-dispersive X-ray

spectroscopy (EDS) detector. Synchrotron X-ray fluorescence (XRF) and High energy X-ray diffraction (HEXRD) experiments on the electrode laminates were carried out at the beamline 2-ID-E and 11-ID-C of the Advanced Photon Source (APS) of Argonne National Laboratory, respectively. Details of the XRF and HEXRD experiments are described in our pervious papers.[18] XPS was carried out on Thermofisher Scientific K-Alpha X-ray Photoelectron Spectrometer (XPS) System using Al K-alpha source (1486.7 eV) at 12 kV and 3 mA (36 W) with a beam spot size of 400 μm.

Charge-discharge tests were conducted on CR2032-type coin cells on a MACCOR series 4000 battery tester at room temperature (ca. 25 ºC). A home-build high-precision leakage current measuring system (based on Keithley 2401 source meters) was used to obtain the leakage current.[2, 24] Electrochemical impedance spectroscopy (EIS) spectra of the half-cells at 4.4 V vs. Li/Li^+ were obtained during the C/10 cycling (2.8-4.4 V vs. Li/Li^+) similar to our previous studies.[18, 25] Zview software was used for spectra fitting.

Results and Discussions

Since we believe minimizing the parasitic reactions between the delithiated NMC electrode and the non-aqueous electrolyte is the key approach to improve the durability of Ni-rich NMCs under high-voltage cycling, here the surface-modified NMC 622 was utilized as a model system to demonstrate our design philosophy. Commercial NMC materials are spherical-shaped particles consisting of densely packed primary particles in order to increase the packing density of the active material and enhance the volumetric energy density of the electrodes. Figures 1a shows the SEM images of a NMC particle in the un-modified electrode laminate. The secondary particle size is around 8-10 μm, the introduction of TiO_2 did not change the particle shape nor particle size (Figure S1). More detailed investigations were focused on the difference

in morphology between the modified and bare samples. Figures 1b-f show the high magnification SEM images of the primary particles. Overall, the primary particles of the NMC are pellet-shaped with ca. 500 nm in length. The surface roughness of the primary particle increased with the number of ALD cycles. Both ALD-20 (Figure 1c) and ALD-40 (Figure 1d) samples exhibited surface features similar to the bare sample (Figure 1b). By increasing the number of ALD cycles, small "islands" were observed (Figures 1e and f), implying the growth of TiO_2 occurred at certain sites on the NMC surface. This agrees with the working mechanisms of ALD process that the introduced metal atoms react with two naturally existing surface hydroxyl (-OH) groups on the NMC surface (see supporting information for reactions involving TiO_2 deposition).

XPS was used to confirm the surface chemistry of the modified electrodes. Figures 2a-c compare the Ni 2p, Mn 2p, and Co 2p spectra of the modified and bare samples. In general, no obvious peak shift occurred after the ALD process. Some minor differences in the area-intensity of the XPS spectra were observed in terms of Ni 2p and Co 2p for samples before and after the surface modification. This may indicate some minor chemical change of the NMC surface through TiO_2. More importantly, Figures 2d and e compare the Ti 2p and O 1s spectra of the samples. Because of the low concentration of Ti on the sample surface, the intensity of the Ti 2p peaks were very low, resulting in a smaller signal-to-noise ratio. Nevertheless, the identification of Ti $2p_{3/2}$ and Ti $2p_{1/2}$ at 459 and 464 eV, respectively, confirmed the existence of TiO_2 on the modified electrode. Together with the significant increase of the metal oxide portion of the O 1s peak (Figure 1f), we believe that TiO_2 was successfully deposited on the NMC surface.

Since the ALD was performed on the surface of the whole electrode laminates, we expect the surface modification should be performed not only on the active NMC material but also other

inactive materials like carbon black. To further confirm this uniform distribution of TiO_2 on the electrodes, synchrotron XRF imaging was used to trace the distribution of Ti. Figure 3a shows the elemental mapping of Ti, Ni, Mn, and Co for the modified electrode. The concentrations of the transition metal elements were much higher, giving them stronger signals. From the mapping of transition metal elements, spherical NMC secondary particles were observed. Conversely, Ti showed a uniform distribution on the electrode.

Further analysis was focused on the impact of this surface modification on the crystal structure of NMC. Figure 3b shows the HEXRD patterns of the surface-modified and bare electrodes. Baseline correction (Figure S2) was performed to eliminate the impact of inactive materials (e.g. PVdF binders). In both patterns, the reflection peaks from NMC can be observed for both modified and bare electrodes. Both samples showed well separated (006)/(102) peaks and (108)/(110) peaks, confirming the typical layered structure of α-$NaFeO_2$ with R-3m space group. It should be noted that due to the presence of the Al current collectors, some diffraction peaks of NMC (i.e. 102 and 104) overlapped with the diffraction peaks of Al. However, all the diffraction peaks from NMC remained the same after introducing the TiO_2, suggesting that the ALD process did not alter the crystal structure of the active material. More importantly, no peak from TiO_2 was observed in the modified sample. This may due to the facts that: (a) TiO_2 was amorphous in nature because of the low temperature environment (i.e. 120 °C) used for ALD process; and/or (b) the extremely low thickness/small size of the TiO_2 ranging from sub-nanometers to a few nanometers. In general, the higher the intensity ratio of I(003)/I(104), the lower the cation mixing between Li and Ni.[26] Figure 3c shows the deconvoluted peaks at 2θ of ~3.3°, where (104) peak from NMC and (200) peak from Al were separated such that

I(003)/I(104) ratio of NMC can be calculated. Both samples exhibited similar intensity ratios, implying a comparable degree of cation mixing for NMC before and after the ALD process.

Now we focused on the electrochemical properties of the bare and modified electrodes. The overlapping voltage profiles together with the overlapping differential capacity profiles (Figure S3) indicated that the ALD process did not influence the redox behavior of the transition metals in the active material. However, we believe the deposited TiO_2 can suppress the interfacial parasitic reactions. To validate our hypothesis, a home-built high-precision leakage current measurement system was used to quantify the rate of solvent oxidation at different potentials. Figure 4a shows examples of the obtained current relaxation curves of three exemplary NMC/Li half-cells. In general, all cells showed good reproducibility and high consistence. In this case, the NMC working electrodes were held at a constant potential of 4.4 V vs. Li/Li^+ for 40 hours such that the state of charge (SoC) or the lithium concentration in the working electrode remained unchanged. Therefore, the initial high current values were originated from the charging of the double-layer capacitor and/or the working electrode while the relatively flat region represented any gain of electrons from the oxidation of electrolyte solvent. With increasing the holding time, the measured current decayed to ca. 0.03 μAmg^{-1}. An exponential decay function (inset of Figure 4a) was used to extract the static leakage current values (y_0) from the current relaxation curves and these static leakage current values can be used as quantitative indicators of the rate of the solvent oxidation reaction.

A series of potentiostatic hold experiments were conducted for the NMC/Li half-cells with and without the surface modification from 4.1 V to 4.6 V vs. Li/Li^+ and the obtained y_0 values were plotted in Figure 4b. In general, static leakage current values increased quickly with higher potentials, indicating the severe electrochemical oxidation of electrolyte components at

the surface of the NMC electrode. As expected, all the surface-modified samples exhibited smaller static leakage current values when comparing to the bare electrode. The smaller current values indicate a slower electron-transfer reaction and less solvent oxidation in a unit time. The difference between the y_0 values became smaller when the potential was higher than 4.5 V vs. Li/Li^+ since the nature of the carbonate solvent oxidation has switched from a chemical reaction-dominated behavior to a direct electrochemical oxidation-dominated behavior.[2] In the latter case, we are reaching the electrochemical stability window of the electrolyte system. Nevertheless, the surface modification by ALD of TiO_2 still had some positive effect on lowering the current values at high potentials. Interestingly, all the samples with ALD modification showed almost identical behavior. The oxidation of electrolyte solvent can be successfully mitigated even with only 20 ALD cycles and further increase in the number of ALD cycles did not lower the y_0 values. This suggests that the interfacial parasitic reactions mainly occur on the reactive sites on the NMC surface and these reactive sites were effectively modified by the deposition of TiO_2 even with a low number of ALD cycles. Further increase in the number of ALD cycles only resulted in a growth of TiO_2 on or near the same reactive site area. The results from our potentiostatic hold experiments successfully provides direct evidence on the mitigation of solvent oxidation reactions by the surface modification. The trend of leakage current can be well correlated to the cycling performance of the electrodes. Figures 4c and S4 compares the cycling performance of NMC/Li half-cells with and without the surface modification. A noticeable difference in terms of capacity retention can be observed when the cells were cycled to both 4.4 V and 4.5 V vs. Li/Li^+. ALD of TiO_2 for other layered cathodes (e.g. $LiCoO_2$ etc.) also demonstrates a similar improvement in the capacity retention (Table S1). This enhancement in the capacity retention was also observed for NMC/graphite full-cells as shown in Figure 4d. Both

the half-cell and full-cell results validate our hypothesis that minimizing parasitic reactions is a key approach to achieve durable Ni-rich NMCs.

While the oxidation of solvent always leads to thick cathodic surface films and large impedance growth during cycling, the impedance response of the half-cells at 4.4 V vs. Li/Li^+ were compared (Figure S5). In fact, the surface-modified electrode showed much smaller surface film resistance hike when compared to its bare counterpart. The mitigation of solvent oxidation may result in less surface film passivation. Since the electrochemical oxidation of solvent can also generate a highly acidic chemical environment, leading to the corrosion of the NMC surface and leaching of the transition metal elements, further analysis was focused on the graphite negative electrodes in order to investigate the chemical cross-talk in the full-cells originated from the transition metal dissolution. First, both the NMC positive electrodes and graphite negative electrodes were recovered from the cycled full-cells. EDS elemental mappings of C, F, Mn, Co, and Ni were obtained for the recovered graphite electrodes (Figure 5a). All the three transition metal elements from NMC were detected on the surface of the graphite electrodes with roughly uniform distribution regardless of the NMC electrodes used. However, the concentration of the transition metal elements found on the graphite electrode surface decreased significantly when the modified NMC electrode was used in the full-cell (Figure 5b). This finding agrees well with the cycling performance of the full-cells (Figure 4d). The leaching out of transition metal cations not only can reduce the number of active Li^+ host sites for the positive electrode but also can trap additional cyclable Li^+ on the surface of the negative electrode. Both cases can cause a much faster capacity fade during full-cell cycling. These results effectively demonstrated that by suppressing the parasitic reaction between the NMC positive electrode and the electrolyte, we can successfully reduce the leaching of transition metal cations from NMC and minimize the

chemical cross-talk in full-cells by lowering the concentration of localized H^+ and protic species caused by solvent oxidation.

Interestingly, it also seemed that the mitigation of the parasitic reactions improved the mechanical integrity of the positive electrodes during the extensive cycling. Figure 5c shows the SEM images of the NMC positive electrodes recovered from the cycled full-cells. The protected electrode showed a much smaller degree of particle fragmentation. In contrast, severe intergranular crackings caused clear particle separation and fragmentation for the bare sample. In extreme cases of fragmentation, active materials were lost due to the loss of grain-to-grain connectivity. It has been commonly accepted that intergranular cracks in NMCs are caused by the different crystallographic orientation and slip planes of the NMC primary particles and the anisotropic volume change of NMCs during charge/discharge.[27-33] From the results shown in Figure 5c, we highly suspect that the loss in the mechanical integrity of NMC particles can also be related to the interfacial parasitic reactions between the NMC electrode and the electrolyte in addition to the anisotropic volume change. Since the dissolution of transition metal cations could corrode the NMC surface and create defect sites, the formed defect sites may act as stress-concentration points for crack formation and propagation, ultimately generating new sites exposed to the electrolyte. In that case, the parasitic reactions and cell degradation become self-initiated and self-sustained. Currently, there is a lack of enough direct evidence to correlate the crack formation on the NMC surface with the parasitic reactions, and our future study will focus on identifying and understanding the fundamental relationship between the two topics of research.

Another consequence of the undesired parasitic reactions between the delithiated positive electrode and the non-aqueous electrolyte is the irreversible phase transformation of the NMC.

HEXRD patterns were obtained for the NMC electrodes with and without the ALD treatment recovered from the cycled full-cells (Figure S6). A similar approach was used to estimate the degree of cation mixing by focusing on the intensity ratio of I(003)/I(104) of the NMC. Since both the surface-modified and bare electrode showed identical peak position and peak intensity ratio at the pristine condition (Figure 3c), either one can be used as a reference to differentiate the impact of extensive cycling on the structural disordering. Figure 6a shows the deconvoluted peaks of (003) and (104) for the NMC electrodes. In general, both cycled electrodes showed a shifting of the peaks and a decrease of the I(003)/I(104) intensity ratio, suggesting the formation of rock-salt and/or spinel-like structures. However, a more pronounced peak shifting was observed for the bare electrode after cycling. Its (003) peak shifted towards a lower two-theta angle while its (104) peak shifted towards a higher two-theta angle than the modified electrode. More importantly, the I(003)/I(104) intensity ratio of the modified electrode was slightly higher than the bare electrode after cycling, indicating a lower degree of cation mixing. This enhancement in the structural stability of NMC by the mitigation of the parasitic reactions can also effectively minimize the voltage-fade of the NMC positive electrode under high-voltage cycling. Figures 6b and S7 show the change in the average discharge potentials of the NMC/Li half-cells during cycling. The formation of less electrochemically inactive NiO-type phase ensured a more stable discharge potential of the modified electrode compared to its bare counterpart.

Conclusions

In this work, the surface of NMC 622 electrodes were chemically modified with TiO_2 via ALD. Unlike other simple coating methods, ALD can provide strong chemical bonds between the Ti and reactive sites on the surface of NMC 622. With this approach, we can utilize this

model system to emphasize the importance of mitigating the parasitic reactions between the delithiated NMC electrode and the non-aqueous electrolyte. The coverage of the TiO_2 on the NMC electrodes was confirmed via morphological and elemental analysis. The ALD treatment did not alter the crystal structure of the NMC and the redox behavior of the transition metal cations at pristine conditions. As expected, the surface modification could well mitigate the oxidation of electrolyte solvent at high potentials, minimizing the cathodic surface film resistance hike and improving the cycling stability of NMC 622 in both half-cell and full-cell configurations. The suppression of the parasitic reactions effectively reduced the dissolution of transition metals, mitigated the particle fragmentation, and lowered the degree of cation mixing of the Ni-rich NMC electrodes. These findings successfully support our design philosophy that minimizing the interfacial parasitic reactions by surface modifications is a key approach to improve the durability of Ni-rich NMCs under high-voltage cycling. More importantly, we revealed possible relationship between the interfacial parasitic reactions and the failure mechanisms of Ni-rich NMCs under high potentials. Further studies are highly encouraged for the battery research community to uncover the fundamental connections between the interfacial parasitic reactions and the performance degradation of Ni-rich NMCs towards the next-generation Li-ion batteries.

Supporting Information

The Supporting Information is available free of charge.

Details on the ALD processes; SEM images of the NMC particles with different ALD cycles; HEXRD patterns of pristine and cycled NMC electrodes with and without ALD treatments; voltage profiles, differential capacity profiles, and cycling performance of the NMC/Li half-cells with and without ALD treatments; impedance responses and the

extracted resistance values of the half-cells, variation of average discharge potentials with and without ALD treatments at different cut-off potentials, and summary of electrochemical performance of layer cathodes with surface modifications by ALD-TiO_2.

Acknowledgments

Research at the Argonne National Laboratory was supported from the U. S. Department of Energy (DOE), Office of Energy Efficiency and Renewable Energy, Vehicle Technologies Office. Argonne National Laboratory is operated for DOE Office of Science by UChicago Argonne, LLC, under contract number DE-AC02-06CH11357. The authors also acknowledge the use of the Advanced Photon Source (APS) and the Center for Nanoscale Materials (CNM) that are supported by the U. S. Department of Energy, Office of Science, Office of Basic Energy Sciences, under Contract No. DE-AC02-06CH11357. Support from Tien Duong of the U.S. DOE's Office of Vehicle Technologies Program is gratefully acknowledged. H. Gao would also like to acknowledge the NSERC Canada Postdoctoral Fellowships Program. X. M. and J. C. acknowledge partial support from the Center for Advanced Surface Engineering, under the National Science Foundation Grant No. OIA-1457888 and the Arkansas EPSCoR Program, ASSET III. X. M. and J. C. also appreciate the financial research support from University of Arkansas. X. M. and J. C. further greatly appreciate the use of the Nano & Bio Materials Characterization Facility at the University of Arkansas.

References

1. Noh, H.-J.; Youn, S.; Yoon, C. S.; Sun, Y.-K., Comparison of the Structural and Electrochemical Properties of Layered $Li[Ni_xCo_yMn_z]O_2$ (x = 1/3, 0.5, 0.6, 0.7, 0.8 and 0.85) Cathode Material for Lithium-Ion Batteries. *J. Power Sources* **2013,** *233*, 121-130.

2. Zeng, X.; Xu, G.-L.; Li, Y.; Luo, X.; Maglia, F.; Bauer, C.; Lux, S. F.; Paschos, O.; Kim, S.-J.; Lamp, P.; Lu, J.; Amine, K.; Chen, Z., Kinetic Study of Parasitic Reactions in Lithium-Ion Batteries: A Case Study on $LiNi_{0.6}Mn_{0.2}Co_{0.2}O_2$. *ACS Appl. Mater. Interfaces* **2016,** *8* (5), 3446-3451.

3. Myung, S.-T.; Maglia, F.; Park, K.-J.; Yoon, C. S.; Lamp, P.; Kim, S.-J.; Sun, Y.-K., Nickel-Rich Layered Cathode Materials for Automotive Lithium-Ion Batteries: Achievements and Perspectives. *ACS Energy Letters* **2017,** *2* (1), 196-223.

4. Xu, K., Nonaqueous Liquid Electrolytes for Lithium-Based Rechargeable Batteries. *Chem. Rev.* **2004,** *104* (10), 4303-4418.

5. Xu, K., Electrolytes and Interphases in Li-Ion Batteries and Beyond. *Chem. Rev.* **2014,** *114* (23), 11503-11618.

6. Tarascon, J. M.; Armand, M., Issues and Challenges Facing Rechargeable Lithium Batteries. *Nature* **2001,** *414* (6861), 359-367.

7. Li, C.; Zhang, H. P.; Fu, L. J.; Liu, H.; Wu, Y. P.; Rahm, E.; Holze, R.; Wu, H. Q., Cathode Materials Modified by Surface Coating for Lithium Ion Batteries. *Electrochim. Acta* **2006,** *51* (19), 3872-3883.

8. Ma, T.; Xu, G.-L.; Li, Y.; Wang, L.; He, X.; Zheng, J.; Liu, J.; Engelhard, M. H.; Zapol, P.; Curtiss, L. A.; Jorne, J.; Amine, K.; Chen, Z., Revisiting the Corrosion of the Aluminum Current Collector in Lithium-Ion Batteries. *The Journal of Physical Chemistry Letters* **2017,** *8* (5), 1072-1077.

9. Borodin, O.; Behl, W.; Jow, T. R., Oxidative Stability and Initial Decomposition Reactions of Carbonate, Sulfone, and Alkyl Phosphate-Based Electrolytes. *The Journal of Physical Chemistry C* **2013,** *117* (17), 8661-8682.

10. Wandt, J.; Freiberg, A.; Thomas, R.; Gorlin, Y.; Siebel, A.; Jung, R.; Gasteiger, H. A.; Tromp, M., Transition Metal Dissolution and Deposition in Li-Ion Batteries Investigated by Operando X-ray Absorption Spectroscopy. *J. Mater. Chem. A* **2016,** *4* (47), 18300-18305.

11. Zhan, C.; Lu, J.; Jeremy Kropf, A.; Wu, T.; Jansen, A. N.; Sun, Y.-K.; Qiu, X.; Amine, K., Mn(II) Deposition on Anodes and Its Effects on Capacity Fade in Spinel Lithium Manganate–Carbon Systems. *Nat. Commun.* **2013,** *4*, 2437.

12. Abraham, D. P.; Twesten, R. D.; Balasubramanian, M.; Petrov, I.; McBreen, J.; Amine, K., Surface Changes on $LiNi_{0.8}Co_{0.2}O_2$ Particles During Testing of High-Power Lithium-Ion Cells. *Electrochem. Commun.* **2002,** *4* (8), 620-625.

13. Abraham, D. P.; Twesten, R. D.; Balasubramanian, M.; Kropf, J.; Fischer, D.; McBreen, J.; Petrov, I.; Amine, K., Microscopy and Spectroscopy of Lithium Nickel Oxide-Based Particles Used in High Power Lithium-Ion Cells. *J. Electrochem. Soc.* **2003,** *150* (11), A1450-A1456.

14. Hwang, S.; Chang, W.; Kim, S. M.; Su, D.; Kim, D. H.; Lee, J. Y.; Chung, K. Y.; Stach, E. A., Investigation of Changes in the Surface Structure of $Li_xNi_{0.8}Co_{0.15}Al_{0.05}O_2$ Cathode Materials Induced by the Initial Charge. *Chem. Mater.* **2014,** *26* (2), 1084-1092.

15. Lin, F.; Markus, I. M.; Nordlund, D.; Weng, T.-C.; Asta, M. D.; Xin, H. L.; Doeff, M. M., Surface Reconstruction and Chemical Evolution of Stoichiometric Layered Cathode Materials for Lithium-Ion Batteries. *Nat. Commun.* **2014,** *5*, 3529.

16. Li, J.; Liu, H.; Xia, J.; Cameron, A. R.; Nie, M.; Botton, G. A.; Dahn, J. R., The Impact of Electrolyte Additives and Upper Cut-off Voltage on the Formation of a Rocksalt Surface Layer in $LiNi_{0.8}Mn_{0.1}Co_{0.1}O_2$ Electrodes. *J. Electrochem. Soc.* **2017,** *164* (4), A655-A665.

17. Jung, S.-K.; Gwon, H.; Hong, J.; Park, K.-Y.; Seo, D.-H.; Kim, H.; Hyun, J.; Yang, W.; Kang, K., Understanding the Degradation Mechanisms of $LiNi_{0.5}Co_{0.2}Mn_{0.3}O_2$ Cathode Material in Lithium Ion Batteries. *Adv. Energy Mater.* **2014,** *4* (1), 1300787-n/a.

18. Gao, H.; Zeng, X.; Hu, Y.; Tileli, V.; Li, L.; Ren, Y.; Meng, X.; Maglia, F.; Lamp, P.; Kim, S.-J.; Amine, K.; Chen, Z., Modifying the Surface of High Voltage Lithium-Ion Cathode. *ACS Applied Energy Materials* **2018,** 1(5), 2254-2260.

19. Li, X.; Liu, J.; Meng, X.; Tang, Y.; Banis, M. N.; Yang, J.; Hu, Y.; Li, R.; Cai, M.; Sun, X., Significant Impact on Cathode Performance of Lithium-Ion Batteries by Precisely Controlled Metal Oxide Nanocoatings via Atomic Layer Deposition. *J. Power Sources* **2014,** *247*, 57-69.

20. Zhang, X.; Belharouak, I.; Li, L.; Lei, Y.; Elam, J. W.; Nie, A.; Chen, X.; Yassar, R. S.; Axelbaum, R. L., Structural and Electrochemical Study of Al_2O_3 and TiO_2 Coated $Li_{1.2}Ni_{0.13}Mn_{0.54}Co_{0.13}O_2$ Cathode Material Using ALD. **2013,** *3* (10), 1299-1307.

21. Bloom, I.; Trahey, L.; Abouimrane, A.; Belharouak, I.; Zhang, X.; Wu, Q.; Lu, W.; Abraham, D. P.; Bettge, M.; Elam, J. W.; Meng, X.; Burrell, A. K.; Ban, C.; Tenent, R.; Nanda, J.; Dudney, N., Effect of Interface Modifications on Voltage Fade in $0.5Li_2MnO_3 \cdot 0.5LiNi_{0.375}Mn_{0.375}Co_{0.25}O_2$ Cathode Materials. *J. Power Sources* **2014,** *249*, 509-514.

22. Cheng, H.-M.; Wang, F.-M.; Chu, J. P.; Santhanam, R.; Rick, J.; Lo, S.-C., Enhanced Cycleabity in Lithium Ion Batteries: Resulting from Atomic Layer Depostion of Al_2O_3 or TiO_2 on $LiCoO_2$ Electrodes. *The Journal of Physical Chemistry C* **2012,** *116* (14), 7629-7637.

23. Meng, X.; Banis, M. N.; Geng, D.; Li, X.; Zhang, Y.; Li, R.; Abou-Rachid, H.; Sun, X., Controllable Atomic Layer Deposition of One-Dimensional Nanotubular TiO2. *Appl. Surf. Sci.* **2013,** *266*, 132-140.

24. Gao, H.; Xiao, L.; Plümel, I.; Xu, G.-L.; Ren, Y.; Zuo, X.; Liu, Y.; Schulz, C.; Wiggers, H.; Amine, K.; Chen, Z., Parasitic Reactions in Nanosized Silicon Anodes for Lithium-Ion Batteries. *Nano Lett.* **2017,** *17* (3), 1512-1519.

25. Gao, H.; Maglia, F.; Lamp, P.; Amine, K.; Chen, Z., Mechanistic Study of Electrolyte Additives to Stabilize High-Voltage Cathode-Electrolyte Interface in Lithium-Ion Batteries. *ACS Appl. Mater. Interfaces* **2017,** *9* (51), 44542-44549.

26. Ohzuku, T.; Ueda, A.; Nagayama, M.; Iwakoshi, Y.; Komori, H., Comparative Study of $LiCoO_2$, $LiNi_{1/2}Co_{1/2}O_2$ and $LiNiO_2$ for 4 Volt Secondary Lithium Cells. *Electrochim. Acta* **1993,** *38* (9), 1159-1167.

27. Lee, E.-J.; Chen, Z.; Noh, H.-J.; Nam, S. C.; Kang, S.; Kim, D. H.; Amine, K.; Sun, Y.-K., Development of Microstrain in Aged Lithium Transition Metal Oxides. *Nano Lett.* **2014,** *14* (8), 4873-4880.

28. Miller, D. J.; Proff, C.; Wen, J. G.; Abraham, D. P.; Bareño, J., Observation of Microstructural Evolution in Li Battery Cathode Oxide Particles by In Situ Electron Microscopy. *Adv. Energy Mater.* **2013,** *3* (8), 1098-1103.

29. Yoon, W.-S.; Chung, K. Y.; McBreen, J.; Yang, X.-Q., A Comparative Study on Structural Changes of $LiCo_{1/3}Ni_{1/3}Mn_{1/3}O_2$ and $LiNi_{0.8}Co_{0.15}Al_{0.05}O_2$ During First Charge Using in situ XRD. *Electrochem. Commun.* **2006,** *8* (8), 1257-1262.

30. Kim, H.; Kim, M. G.; Jeong, H. Y.; Nam, H.; Cho, J., A New Coating Method for Alleviating Surface Degradation of $LiNi_{0.6}Co_{0.2}Mn_{0.2}O_2$ Cathode Material: Nanoscale Surface Treatment of Primary Particles. *Nano Lett.* **2015,** *15* (3), 2111-2119.

31. Mukhopadhyay, A.; Sheldon, B. W., Deformation and Stress in Electrode Materials for Li-Ion Batteries. *Progress in Materials Science* **2014,** *63*, 58-116.

32. Zhou, Y.-N.; Ma, J.; Hu, E.; Yu, X.; Gu, L.; Nam, K.-W.; Chen, L.; Wang, Z.; Yang, X.-Q., Tuning Charge–Discharge Induced Unit Cell Breathing in Layer-Structured Cathode Materials for Lithium-Ion Batteries. *Nat. Commun.* **2014,** *5*, 5381.

33. Dolotko, O.; Senyshyn, A.; Mühlbauer, M. J.; Nikolowski, K.; Ehrenberg, H., Understanding Structural Changes in NMC Li-Ion Cells by in situ Neutron Diffraction. *J. Power Sources* **2014,** *255*, 197-203.

List of Figures

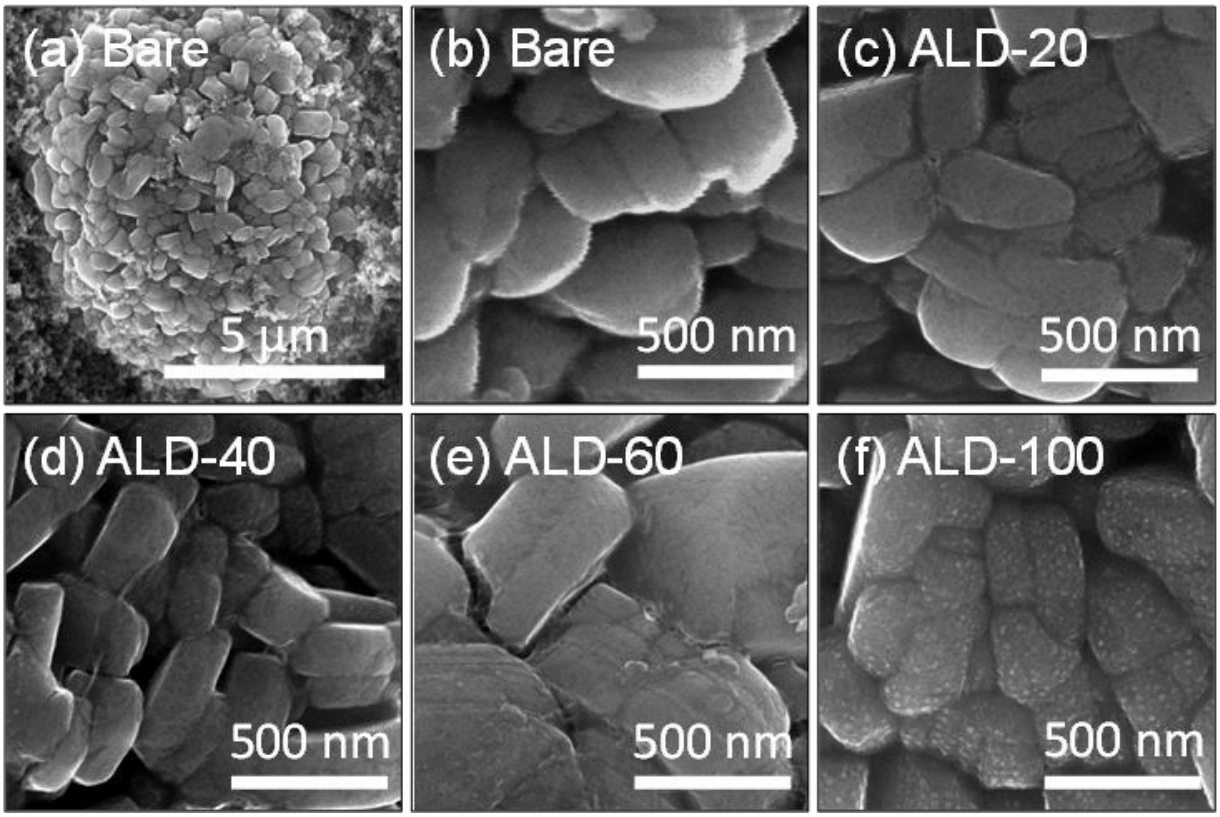

Figure 1. SEM images of (a, b) a bare NMC 622 particle without any surface modifications at different magnifications, and high magnification SEM images of surface-modified NMC 622 particles with (c) 20 ALD cycles, (d) 40 ALD cycles, (e) 60 ALD cycles, and (f) 100 ALD cycles.

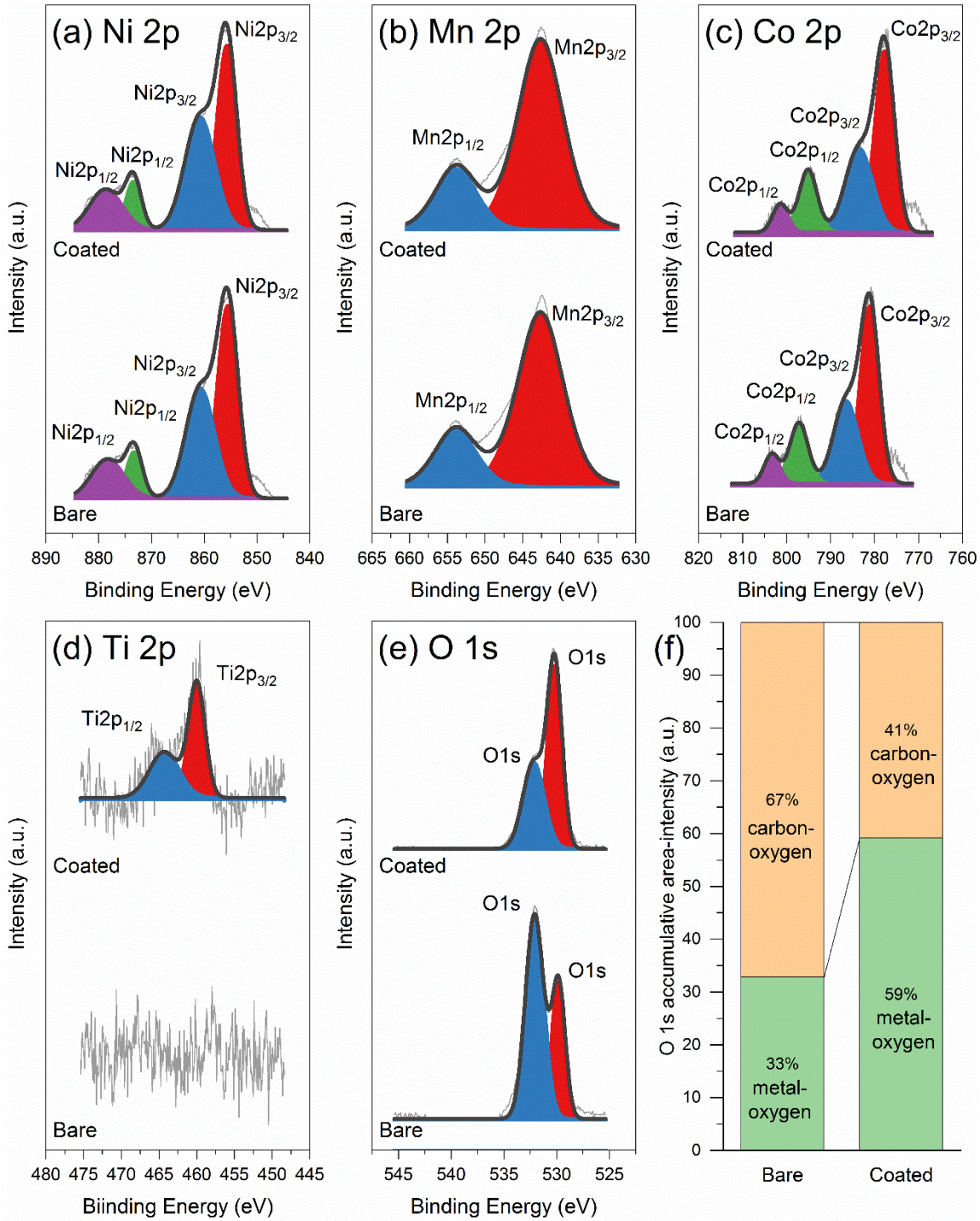

Figure 2. (a) Ni 2p, (b) Mn 2p, (c) Co 2p, (d) Ti 2p, (e) O 1s XPS spectra for the surface-modified electrodes with 20 ALD cycles and bare electrodes and (f) O1s accumulative area-intensity ratio comparison between the bare and 20 ALD cycles-treated electrodes.

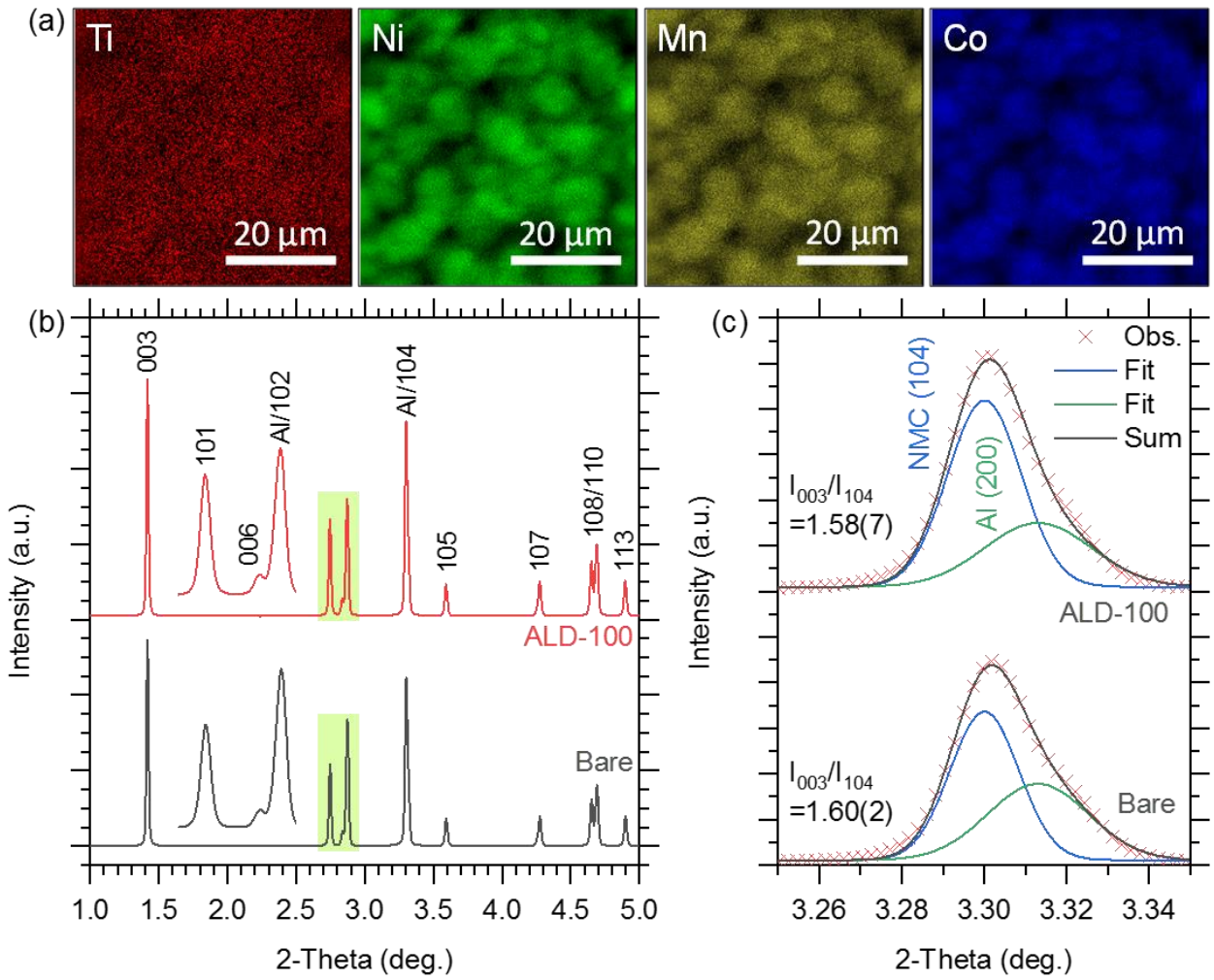

Figure 3. (a) XRF elemental mapping of the 20 ALD cycles-treated NMC electrodes for Ti, Ni, Mn, and Co, (b) HEXRD patterns of the 100 ALD cycles-treated and bare NMC electrodes at pristine condition, and (c) deconvolution of the overlapping diffraction peaks from both NMC and Al current collectors for the two samples.

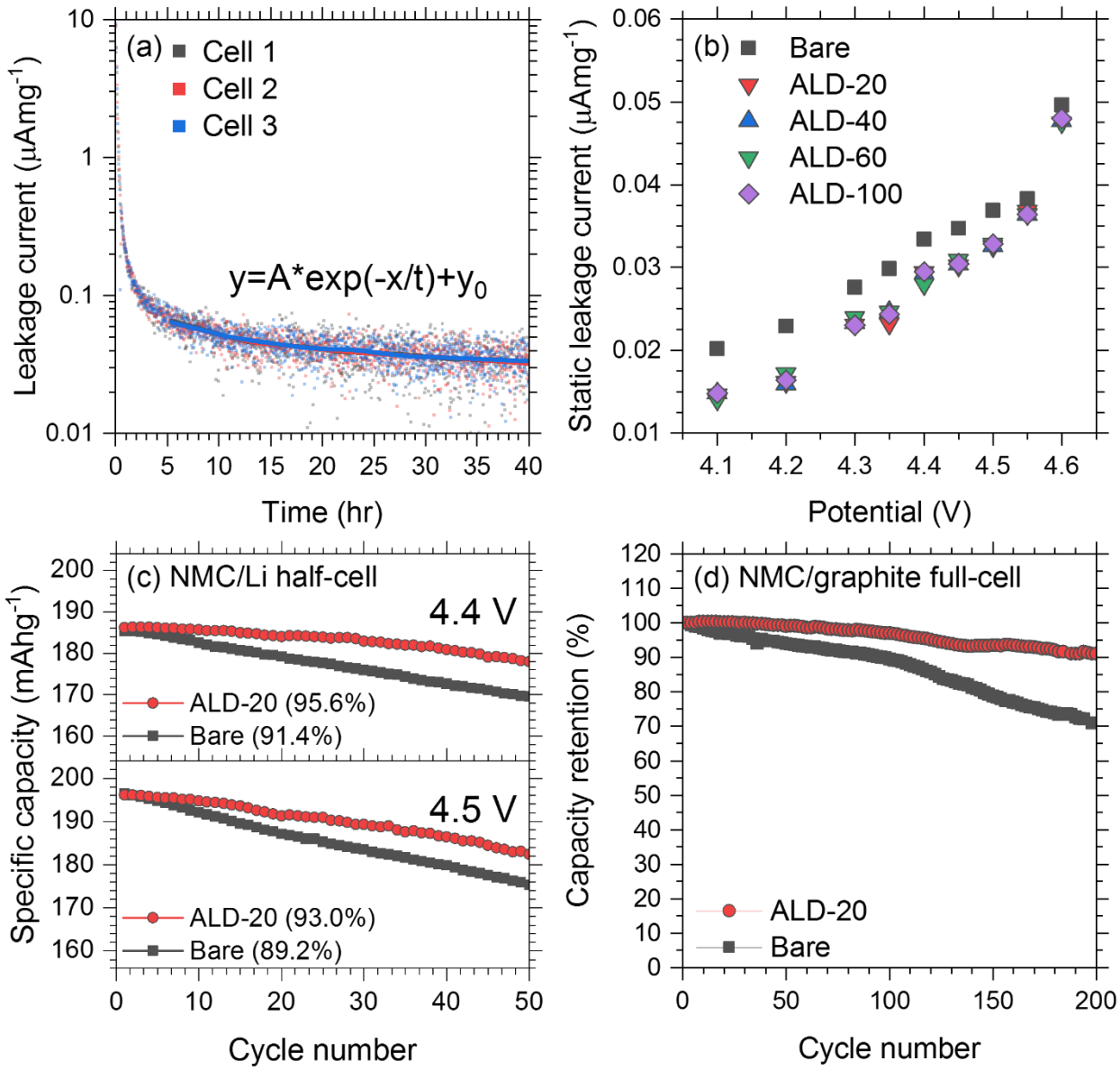

Figure 4. (a) Typical current relaxation curves collected from NMC/Li half-cells during potentiostatic hold at 4.4 V vs. Li/Li^+, (b) variation of the static leakage current (y_0) as a function of potential with and without surface modification, (c) cycling performance of NMC/Li half-cells using 20 ALD cycles-treated and bare NMC electrodes at 4.4 V and 4.5 V vs. Li/Li^+ under C/10 current density, (d) cycling performance of NMC/graphite full-cells using 20 ALD cycles-treated and bare NMC electrodes under at 4.45 V vs. Li/Li^+ under C/3 current density.

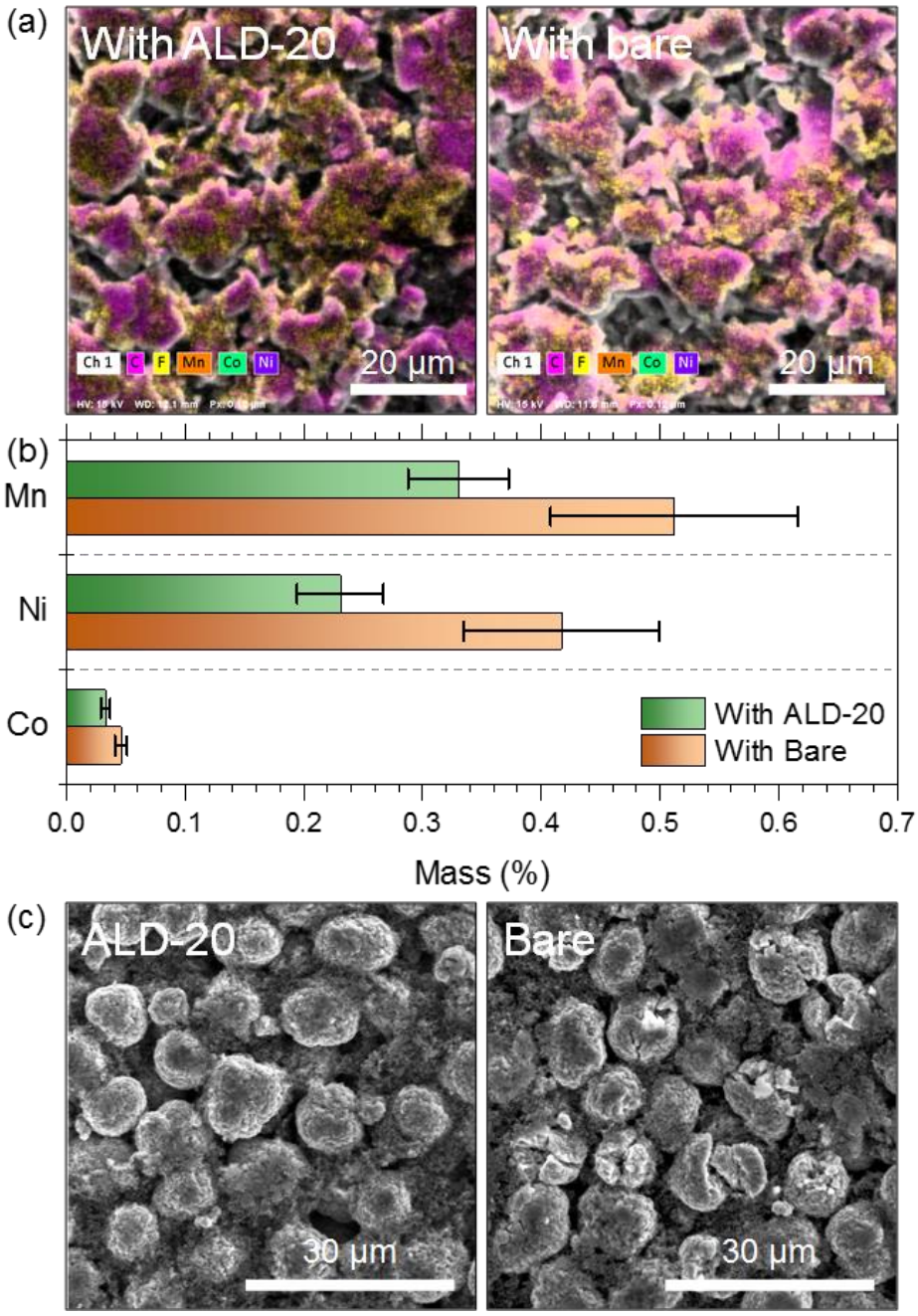

Figure 5. (a) EDS elemental mapping of C, F, Mn, Co, Ni, and (b) quantification of the amount of Mn, Ni, and Co detected on the surface of graphite negative electrodes recovered from cycled NMC/graphite full-cells coupled with and without surface-modified NMC electrodes (two-sigma absolute error), (c) SEM images of the NMC positive electrodes with and without surface modification recovered from cycled NMC/graphite full-cells.

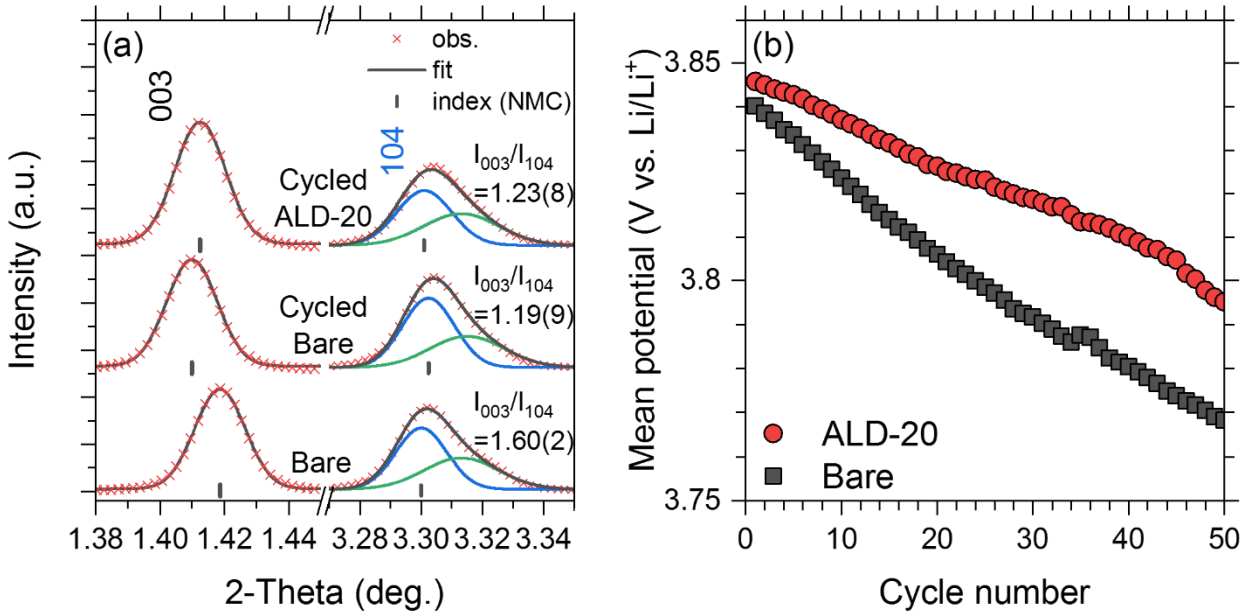

Figure 6. (a) Fitted HEXRD pattern of the cycled NMC electrodes with and without 20 ALD cycle-treatment and their comparison to the pristine bare NMC electrode, (b) variation of average discharge potential of NMC electrodes with and without chemical modifications cycled at 4.4 V vs. Li/Li^+ (C-rate = 0.1).